CSIRO PUBLISHING
www.publish.csiro.au/journals/pasa *Publications of the Astronomical Society of Australia*, 2006, **23**, 106–118

Multivariate Characterization of Hydrogen Balmer Emission in Cataclysmic Variables

Gordon E. Sarty[A,B,D] *and Kinwah Wu*[B,C]

[A] Departments of Psychology and Physics & Engineering Physics, University of Saskatchewan, Saskatoon, Saskatchewan S7N 5A5, Canada
[B] Mullard Space Science Laboratory, University College London, Holmbury St. Mary, Surrey RH5 6NT, UK
[C] TIARA, Department of Physics, National Tsing Hua University, Hsinchu 300, Taiwan
[D] Corresponding author. E-mail: gordon.sarty@usask.ca

Received 2006 April 11, accepted 2006 August 14

Abstract: The ratios of hydrogen Balmer emission line intensities in cataclysmic variables are signatures of the physical processes that produce them. To quantify those signatures relative to classifications of cataclysmic variable types, we applied the multivariate statistical analysis methods of principal components analysis and discriminant function analysis to the spectroscopic emission data set of Williams (1983). The two analysis methods reveal two different sources of variation in the ratios of the emission lines. The source of variation seen in the principal components analysis was shown to be correlated with the binary orbital period. The source of variation seen in the discriminant function analysis was shown to be correlated with the equivalent width of the Hβ line. Comparison of the data scatterplot with scatterplots of theoretical models shows that Balmer line emission from T CrB systems is consistent with the photoionization of a surrounding nebula. Otherwise, models that we considered do not reproduce the wide range of Balmer decrements, including 'inverted' decrements, seen in the data.

Keywords: accretion: accretion discs — stars: cataclysmic variables — stars: dwarf novae — stars: emission line — stars: statistics

1 Introduction

Cataclysmic variables (CVs) are semi-detached binaries in which a red (K or M) main-sequence, or slightly evolved, low-mass star loses mass to a white-dwarf primary through overfilling its Roche lobe. They can be divided into two groups, the magnetic CVs (mCVs) and the non-magnetic CVs, according to whether the white-dwarf has a magnetic field that is strong enough to affect the accretion dynamics. Semi-detached binaries frequently possess an accretion disc, where gravitational energy is converted to kinetic energy and then to radiation. With mCVs the magnetic-field strength of the white-dwarf is high enough to disrupt the accretion disc at the magnetosphere. The white-dwarf's magnetosphere will determine the inner radius of the accretion disc and the tidal force exerted by the secondary star will truncate the outer region of the disc. If the magnetosphere is large enough, no disc will form.

MCVs without an accretion disc are known as polars (or AM Herculis systems). In a polar the white-dwarf magnetic field is sufficiently strong ($\sim$10 MG) to also lock the white-dwarf and its companion star into synchronous (or almost synchronous) rotation with the binary orbit. The accretion flow near the white-dwarf is channelled by the field and a shock is often formed near the base of the accretion column before the accreting gas settles onto the white-dwarf atmosphere. The shock heats the accreting gas, leading to the emission of bremsstrahlung X-rays that can subsequently photoionize the cooler gas upstream. For systems consisting of a white-dwarf with a moderately strong magnetic field ($\sim$1 MG), the white-dwarf spin and the orbital motion are not synchronous, although the secondary may still be tidally locked and rotate with the orbit. These moderately magnetic systems are known as intermediate polars (IPs). Most IPs possess an accretion disc, but the inner region of the disc is truncated by the magnetic field, and the flow is channelled in the white-dwarf magnetosphere, similar to polars. A shock can be formed in the accretion column, and the X-rays from the post-shock region can photoionize both the pre-shock gases in the accretion column and the cool gas in the accretion disc. It is worth noting that some IPs may not have a fully developed accretion disc. They probably have a thin accreting annulus, which couples loosely to the magnetosphere of the white-dwarf.

Non-magnetic CVs form a heterogeneous class of objects, which include nova, dwarf nova and nova-like systems, primarily on the basis of their light curve behaviour (although strict classification is sometimes not possible, e.g. some novae are also polars). They are asynchronously rotating systems, and they have a fully

 10.1071/AS06011 0727-3061/05/02144

developed accretion disc with an inner edge extending to the white-dwarf surface. A substantial fraction of the accretion energy is dissipated in a transition layer between the disc and the white-dwarf. The strong UV photons emitted from the transition region can be a main cause of photoionization in the accreting gas.

CVs are strong emission line objects, particularly in quiescence. They all show clear H Balmer emission sequences. He I, He II, and high ionization lines of other species are also prominent in the optical spectra of many systems. The high ionization lines of the CVs are believed to be emission from photoionized gas in the accretion disc (for IPs and non-magnetic CVs), the accretion stream, or irradiatively heated surface of the companion star. Some of the lines may originate from hot spots in the system, for example in regions where the accretion stream impacts onto the accretion disc and where the accretion flow begins to couple with the magnetic field. In these cases the gas is often heated by shocks that are formed as consequence of an abrupt change in the dynamics of the accretion flow. (For reviews of CVs and related accretion physics, see Warner 1995; Cropper 1990; Wu 2000; Wu et al. 2003).

The lines from photoionized gases and shock heated gases have different properties. An example is that of the relative strengths of the H Balmer emission lines. For instance, simple photoionization-recombination models (Osterbrock 1989) generally predict ratios of ≈ 3.5 for Hα/Hβ, yet observations show Hα/Hβ which deviate significantly from these model predictions. Such deviation implies that the line formation process is more complex than simple photoionization and subsequent recombination.

Here we analyze the H Balmer emission from CVs systematically using multivariate statistical methods. We consider the systems in Williams (1983) as the sample for our analysis. We search for correlations between the emission line ratios and CV classification and review the line formation mechanisms that may be responsible for the correlations. The paper is organized as follows. In Section 2 we review the multivariate statistical methods used to analyze the H Balmer emission data. These methods are discriminant function and principal component analysis. In Section 3 we present the data in a four dimensional scatterplot space and give the results of the discriminant function and principal component analysis in that geometric space. We also review models of Balmer emission relevant to CVs. In Section 4 we discuss possible physical causes, based on existing models, of the statistical behaviour of the data. Two significant directions of variation are found that correlate with the binary orbital period and the equivalent width of the Hβ line. Our conclusions are given in Section 5.

2 Statistical Methods

We consider the systems listed in Williams (1983) as our sample. The spectra were obtained in 1980 or 1981 using the 1.3-m telescope at McGraw–Hill Observatory. As the data were collected with the same telescope/instruments and were reduced in a similar manner, this ensures that any variations present are less likely to be caused by different experimental settings and data analysis procedures. The emission line ratios Hα/Hβ, Hγ/Hβ, Hδ/Hβ, and Hε/Hβ were derived from the spectroscopic data presented in Williams (1983) and represent integrated line intensities above the continuum. Only systems for which all four H Balmer emission lines were measured were retained, and sources since identified as non-CVs or which were not listed in Downes et al. (2001) (TU Leo, Z And, HK Sco, and CL Sco) were discarded. The remaining data (representing 95 of 153 original spectra) are reproduced in Table 1 along with four classification schemes. None of the systems considered here were in outburst when the data were taken. There are three observations of two AM CVn stars which have very little hydrogen. However, the AM CVn data were retained because their H Balmer line ratios were reported. We have also not given multiple observations of a single star any special status in our analysis, assuming, as a first approximation, that the data represent a random sample from the observable CVs.

Of the classification schemes considered, the first classification is that from the Atlas of CVs: The Living Edition (Downes et al. 2001) as of 2005 February. Based on the Downes et al. classification, three other, simpler, classification schemes were produced. For classification scheme Class 1, the sources were grouped into one of four groups: (a) dwarf novae, (b) polar & IP (i.e. mCVs), (c) nova & nova-like, and (d) double degenerate (double degenerate systems contain two white-dwarfs instead of a white-dwarf and a red dwarf). All sources classified as DQ Herculis systems were put in the polar & IP (mCV) group unless the DQ Her classification was listed as very uncertain. The results of a discriminant function analysis (see below) of the groups in Class 1 lead to the definition of the groups in Class 2. That is, the groups of Class 2 were determined by a statistical analysis of the physically distinct groups of Class 1. For classification scheme Class 2 the sources were split into two groups, (a) dwarf nova and (b) other, based on the grouping of Class 1. For classification scheme Class 3 the sources were split into two groups, (a) dwarf nova and (b) mCVs, based on the grouping of Class 1, which excluded the nova & nova-like and the double degenerate groups. The grouping of Class 3 was defined in an attempt to find statistical differences between objects that are similar but for the magnetic field of the primary.

Discriminant functions were constructed, using the SPSS statistical software (SPSS Inc., Chicago, USA), to maximally separate the two groups of Class 2 and Class 3. The discriminant functions were of the form

$$z = c_0 + \sum_{i=1}^{4} c_i x_i \qquad (1)$$

where x_i are the emission line ratios and c_i are coefficients such that the values of z for the centroids

Table 1. Balmer line emission data as taken from Williams (1983) together with the classifications used in the discriminant function analysis.

Star[A]	Hα/Hβ	Hγ/Hβ	Hδ/Hβ	Hε/Hβ	ACV[B] Class	Class[C–E] 1	2	3	EW(β)[F] [Å]	DW(β)[G] [km s^{-1}]	P_{orb}[H] [days]
V368 Aql	0.98	0.92	0.87	0.85	na	N&NL	O				0.3452
V603 Aql	0.49	1.33	1.50	1.70	na/dq::	N&NL	O		7.7		0.1385
V603 Aql	0.44	1.22	1.43	1.55	na/dq::	N&NL	O		6.2		0.1385
DN Gem	0.53	1.17	1.43	1.58	na	N&NL	O		8.4	562	0.12785
DQ Her	0.79	1.13	1.35	1.30	na/dq	P&IP	O	M	33.3	505	0.193621
DQ Her	0.59	1.09	1.26	1.30	na/dq	P&IP	O	M	16.7	519	0.193621
DQ Her	0.59	1.13	1.21	1.26	na/dq	P&IP	O	M	20.5	460	0.193621
V533 Her	0.43	1.29	1.62	1.64	na	N&NL	O		4.9	396	0.147
DI Lac	0.58	1.13	1.30	1.22	na	N&NL	O				0.543773
HR Lyr	0.52	1.25	1.37	1.43	na	N&NL	O				
BT Mon	0.75	1.04	1.08	1.08	na	N&NL	O		23.3	343	0.338814
BT Mon	0.92	0.99	0.96	0.93	na	N&NL	O		35.0	592	0.338814
BT Mon	0.87	1.04	1.08	1.09	na	N&NL	O		30.6	644	0.338814
V841 Oph	0.78	1.05	1.17	1.13	nb	N&NL	O		1.6		0.6014
GK Per	1.25	0.71	0.65	0.62	na/dq	P&IP	O	M	10.8	309	1.9968
X Ser	0.56	1.06	1.37	1.17	nb:	N&NL	O		7.1		1.48
T CrB	2.97	0.65	0.46	0.29	nra	N&NL	O				227.5687
RS Oph	3.37	0.60	0.43	0.43	nra	N&NL	O		12.7		455.72
T Pyx	0.56	1.24	1.41	1.50	nrb	N&NL	O		9.7	554	0.076223
V1017 Sgr	1.42	0.47	0.50	0.34	nb	N&NL	O				5.714
RX And	0.84	1.16	1.21	1.30	ugz	DN	DN	DN	58.3	664	0.209893
RX And	0.54	1.52	1.77	1.79	ugz	DN	DN	DN			0.209893
AR And	0.97	1.26	1.29	1.63	ug	DN	DN	DN	38.5	702	0.163
AR And	0.84	1.16	1.63	1.71	ug	DN	DN	DN	39.2	379	0.163
UU Aql	0.97	1.05	1.20	1.24	ug	DN	DN	DN	50.4	454	0.163532
UU Aql	0.97	1.16	1.39	1.55	ug	DN	DN	DN	80.9	670	0.163532
SS Aur	1.06	1.20	1.27	1.50	ug	DN	DN	DN			0.1828
SS Aur	1.13	1.08	1.16	1.37	ug	DN	DN	DN	122.0	569	0.1828
FS Aur	0.83	1.12	1.25	1.45	ug	DN	DN	DN	60.8	903	0.0595
FS Aur	0.86	1.06	1.14	1.38	ug	DN	DN	DN	35.3	571	0.0595
Z Cam	0.48	1.17	1.36	1.56	ugz	DN	DN	DN			0.289841
HT Cas	0.75	1.16	1.26	1.64	ugsu	DN	DN	DN	97.7	943	0.073647
HT Cas	0.78	1.13	1.38	1.72	ugsu	DN	DN	DN	117.0	1032	0.073647
WW Cet	0.96	1.22	1.46	1.70	ugz:	DN	DN	DN	42.7	849	0.1758
WW Cet	0.64	1.13	1.22	1.27	ugz:	DN	DN	DN	25.4	673	0.1758
1E0643.0	0.85	1.08	1.33	1.59	ug/ugz	DN	DN	DN	96.5	776	0.216778
1E0643.0	1.18	0.91	0.82	1.14	ug/ugz	DN	DN	DN	81.3	584	0.216778
1E0643.0	1.02	0.72	0.78	0.86	ug/ugz	DN	DN	DN	43.5	461	0.216778
1E0643.0	0.99	0.96	1.02	1.22	ug/ugz	DN	DN	DN	64.0	506	0.216778
1E0643.0	0.53	1.25	1.47	1.67	ug/ugz	DN	DN	DN	6.1		0.216778
1E0643.0	0.81	1.08	1.13	1.33	ug/ugz	DN	DN	DN	49.1	873	0.216778
SY Cnc	0.73	0.99	1.09	1.09	ugz	DN	DN	DN	13.7	498	0.38
SY Cnc	0.54	1.42	1.56	1.64	ugz	DN	DN	DN			0.38
YZ Cnc	0.72	1.34	1.45	1.70	ugsu	DN	DN	DN	80.1	941	0.0868
YZ Cnc	0.66	1.33	1.58	2.06	ugsu	DN	DN	DN	131.0	906	0.0868
AK Cnc	0.72	1.00	0.91	1.01	ugsu	DN	DN	DN			0.0651
SS Cyg	1.13	0.89	0.92	1.05	ugss	DN	DN	DN	69.5	477	0.27513
SS Cyg	1.05	0.91	0.86	0.97	ugss	DN	DN	DN	67.0	513	0.27513
SS Cyg	0.70	1.18	1.29	1.46	ugss	DN	DN	DN	30.2	786	0.27513
EM Cyg	0.60	1.10	1.33	1.42	ugz	DN	DN	DN	2.6		0.290909
AB Dra	0.59	1.16	1.35	1.50	ugz	DN	DN	DN	19.6	973	0.152
IR Gem	0.77	1.16	1.37	1.60	ugsu	DN	DN	DN	80.6	554	0.0684

AH Her	0.97	0.96	0.98	1.06	ugz	DN	DN	DN	26.5	682	0.258116
EX Hya	0.49	1.16	1.34	1.59	ug/dq	P&IP	O	M	54.4	939	0.068234
EX Hya	0.55	1.12	1.25	1.38	ug/dq	P&IP	O	M	75.2	1492	0.68234
EX Hya	0.61	1.18	1.30	1.39	ug/dq	P&IP	O	M	80.7	1144	0.68234
T Leo	0.60	1.42	1.50	1.54	ugsu	DN	DN	DN	115.0	457	0.05882
X Leo	1.05	1.21	1.38	1.67	ug	DN	DN	DN	22.3	919	0.1644
CN Ori	0.49	1.33	1.54	1.59	ugz	DN	DN	DN			0.163199
CZ Ori	1.05	1.10	1.13	1.37	ug	DN	DN	DN	43.5	503	0.2189
RU Peg	0.60	1.21	2.81	3.35	ugss	DN	DN	DN	4.7		0.3746
WZ Sge	0.47	1.30	1.55	1.71	ugwz/dq	P&IP	O	M	27.8	725	0.056688
SW UMa	0.42	1.35	1.51	1.58	ugsu/dq	P&IP	O	M			0.056815
SW UMa	0.66	1.22	1.41	1.63	ugsu/dq	P&IP	O	M	64.3	657	0.056815
SW UMa	0.68	1.18	1.39	1.55	ugsu/dq	P&IP	O	M	71.6	825	0.056815
TW Vir	0.79	1.21	1.41	1.50	ug	DN	DN	DN	69.8	805	0.18267
TW Vir	0.91	1.26	1.38	1.99	ug	DN	DN	DN	96.5	601	0.18267
TW Vir	0.91	1.21	1.35	1.75	ug	DN	DN	DN	73.3	680	0.18267
AE Aqr	1.30	0.71	0.61	0.52	dq	P&IP	O	M	21.7	369	0.411656
TT Ari	0.44	1.30	1.47	1.57	vy/dq:	P&IP	O	M	7.0		0.13755
G61-29	0.64	1.21	1.42	1.50	ibwd	DD	O				0.032339
AM CVn	0.37	1.43	1.71	1.83	ibwd	DD	O				0.011907
AM CVn	0.37	1.43	1.75	1.93	ibwd	DD	O				0.011907
YY Dra	1.41	1.08	1.18	1.29	dq	P&IP	O	M	129.0	739	0.165374
2A0311-227	1.09	0.96	0.91	0.97	am	P&IP	O	M	43.9	901	0.056266
AM Her	0.98	1.43	1.59	1.84	am	P&IP	O	M	18.4	230	0.128927
AM Her	0.85	1.27	1.39	1.55	am	P&IP	O	M	15.2	232	0.128927
AM Her	0.72	1.26	1.46	1.59	am	P&IP	O	M	55.4	517	0.128927
AM Her	1.01	1.16	1.34	1.47	am	P&IP	O	M	48.8	355	0.128927
V426 Oph	0.66	1.18	1.34	1.45	ugz/dq:	P&IP	O	M	14.9	813	0.2853
V442 Oph	0.54	1.10	1.22	1.25	vy	N&NL	O		4.8	469	0.12433
V2051 Oph	0.60	0.98	1.18	1.35	ugsu	DN	DN	DN	124.0	853	0.062428
VV Pup	0.62	1.25	1.24	1.20	am	P&IP	O	M	93.9	513	
V Sge	0.50	1.25	1.59	1.71	nlv	N&NL	O		52.9	739	0.514197
V Sge	0.61	1.24	1.43	1.62	nlv	N&NL	O		62.2	645	0.514197
N Sgr 1962	1.96	0.85	0.74	0.72	nra	N&NL	O		59.6	208	
RW Tri	0.59	1.17	1.26	1.34	ux	N&NL	O				0.231883
UX UMa	0.47	1.31	1.51	1.79	ux	N&NL	O		4.1	360	0.196671
AN UMa	0.52	1.14	1.22	1.24	am	P&IP	O	M	28.1	783	0.79753
AN UMa	0.51	1.14	1.19	1.36	am	P&IP	O	M	24.2	661	0.79753
2H2215–086	0.58	1.21	1.42	1.42	dq	P&IP	O	M	25.0	382	0.20206
2H2215–086	0.47	1.21	1.33	1.34	dq	P&IP	O	M	27.3	323	0.20206
2H2215–086	0.52	1.21	1.43	1.42	dq	P&IP	O	M	17.6	704	0.20206
2H2252–035	0.47	1.26	1.46	1.51	dq	P&IP	O	M	10.6	582	0.149626
0623+71	0.43	1.37	1.53	1.64	vy	N&NL	O				0.153693

[A] G61–29 = GP Com, YY Dra = DO Dra, 2A0311–227 = EF Eri, N Sgr 1962 = V3890 Sgr, 2H2215–086 = FO Aqr, 2H2252–035 = AO Psc, 0633+71 = BZ Cam.

[B] Atlas of Cataclysmic Variables (ACV) (Downes et al. 2001) nomenclature: ug = U Gem variable (dwarf nova), ugz = U Gem variable (Z Cam subtype), ugss = U Gem variable (SS Cyg subtype), ugsu = U Gem variable (SU UMa subtype), ugwz = U Gem variable (WZ Sge subtype), na = Fast nova, nb = Slow nova, nra = Recurrent nova - giant donor, nrb = Recurrent nova - non-giant donor, nlv = Novalike variable (V Sge subtype), ux = Novalike variable (UX UMa subtype), vy = Novalike variable (VY Scl subtype - systems which undergo low states), am = AM Herculis variable (synchronous rotators), dq = DQ Herculis variable (non-synchronous rotators), ibwd = Interacting binary white-dwarf, : = Uncertain, :: = Very uncertain.

[C] DN = dwarf nova, P&IP = polar and IP, N&NL = nova and NL, DD = double degenerate.

[D] DN = dwarf nova, O = other.

[E] DN = dwarf nova, M = magnetic.

[F] EW = equivalent width.

[G] DW = Doppler width.

[H] Orbital period data from Downes et al. (2001).

(mean) of the two groups are maximally different (c_0 is arbitrary). Specifically we used x_1 to represent Hα/Hβ, x_2 to represent Hγ/Hβ, x_3 to represent Hδ/Hβ, and x_4 to represent Hε/Hβ. Discriminant functions may be used to quantify the separation of more than two groups; we originally computed a discriminant function for the classification scheme of Class 1 but found significant separations only for the groups subsequently defined in Class 2 and 3. The statistical significance of the discriminant function was characterized with Wilk's Λ, a statistic that generalizes Fisher's analysis of variance F statistic to the multivariate situation, and an associated p-value that gives the probability of incorrectly rejecting the null hypothesis of no difference between the two groups. The null hypothesis is generally rejected and statistically significant differences are said to be found when $p < 0.05$. The discriminant function test of two group separation on the basis of the multivariate line ratio data is mathematically equivalent, under the assumption of normal homoscedasticity (which means that all groups are assumed to be multivariate normally distributed with the same covariance matrices), to Hotelling's T^2 test. The T^2 statistic tests if the mean vectors of two groups are significantly different and is equivalent to Λ because T^2 and Λ give the same likelihood ratio test with two groups (Rencher 2002). Histograms, along with the best fit normal distribution, of the discriminant function values were plotted to show the group separation provided by the discriminant function. To aid in the interpretation of the resulting discriminant functions a principal component analysis (PCA) was also conducted.

PCA finds the best description of the data in scatterplot space assuming they are a sample from a multivariate normal population (Rencher 2002). Surfaces of constant σ (standard deviation from the mean vector) of a multivariate normal distribution form ellipsoids in scatterplot space. So PCA finds an ellipsoid in scatterplot space such that the major axis of the ellipsoid lies in the direction of maximum variation of the data; this is the first principal component direction. Subsequent principal component directions are directions of maximal variation that are geometrically orthogonal to the previous principal component directions. The ellipsoid is the geometrical expression of the data's covariance matrix—the eigenvalues and eigenvectors of the covariance matrix define the size and direction of the ellipsoid. It should be noted that PCA considers all the data to be coming from a single multivariate normally distributed population with one mean vector while discriminant functions assume that each group comes from its own population with different mean vectors (but the covariance matrices of each population are assumed equal). The discriminant function's level surfaces will generally contain the principal axes of the individual group ellipsoids (since they are the same, except translated, under the assumption of homoscedasticity) to achieve maximal group separation. From this it can be seen that the normal to the discriminant function's level surfaces should be roughly perpendicular to the PCA's first component direction defined from the ellipsoid that considers all the data together.

For comparison to the data, scatterplots of H Balmer emission line ratios from accretion discs predicted by theoretical models were constructed. Four models were considered. The first is the optically thin nebula model (Osterbrock 1989), which assumes that the line formation is dominated by photoionization–recombination. The second model considered the temperature and density distribution in the accretion disc explicitly via an α-disc prescription (Shakura & Sunyaev 1973). The line calculations were carried out assuming a local thermodynamic equilibrium (LTE) condition with emission primarily from the outer region of the disc, which is optically thin to the continuum emission (Williams 1980). The third model assumed that the emission region is isothermal and employed a non-LTE radiative transfer formulation (Williams 1991) in the line calculations. Finally we considered the chromospheric models of Williams (1995) where a hot, photoionized chromosphere above the accretion disc is modelled.

3 Analysis

3.1 Observed Properties of H Lines in the CV Samples

The scatterplot of the emission line ratio data from Table 1 is shown in Figure 1. It may be discerned that the data tend to fall on a line in the 4D scatterplot space. Visible in the scatterplot are some obviously outlying systems. Those systems are as follows. RS Oph is a recurrent nova with past outbursts observed in 1898, 1933, 1958, 1967, 1985, and 2006, T CrB is a recurrent nova with past outbursts observed in 1866 and 1946, and N Sgr 1962 (V3890 Sgr) is a recurrent nova with past outbursts observed in 1962 and 1990. RS Oph, T CrB and V3890 Sgr are all of the T CrB subclass of recurrent nova which have M giant secondaries, $P_{\rm orb} \gtrsim 100$ d and a high rate of mass accretion, $M_1 \gtrsim 1 \times 10^{-8}\ {\rm M}_\odot\ {\rm yr}^{-1}$, onto a white-dwarf primary whose mass is close to the Chandrasekhar mass (Warner 1995). There are no other T CrB type systems in the data set. Duerbeck (1987) lists V1017 Sgr as a possible symbiotic star or recurrent nova. RU Peg is a U Gem type of dwarf nova with no other known characteristics that would suggest that it is different from other dwarf novae.

The discriminant function that maximally splits the Class 2 groups of dwarf novae versus others is

$$z = 1.799 - 0.152x_1 - 1.927x_2 - 9.714x_3 + 9.226x_4 \quad (2)$$

The value of Wilk's lambda for this function is Λ = 0.729 with $p = 9 \times 10^{-6}$. The unit vector $\mathbf{V}_2$ = [–0.011 –0.142 –0.718 0.681]$^{\rm T}$ is normal to the level surface hyperplanes of the discriminant function for Class 2. Histograms of the distribution of the values for the Class 2 discriminant function are shown in Figure 2.

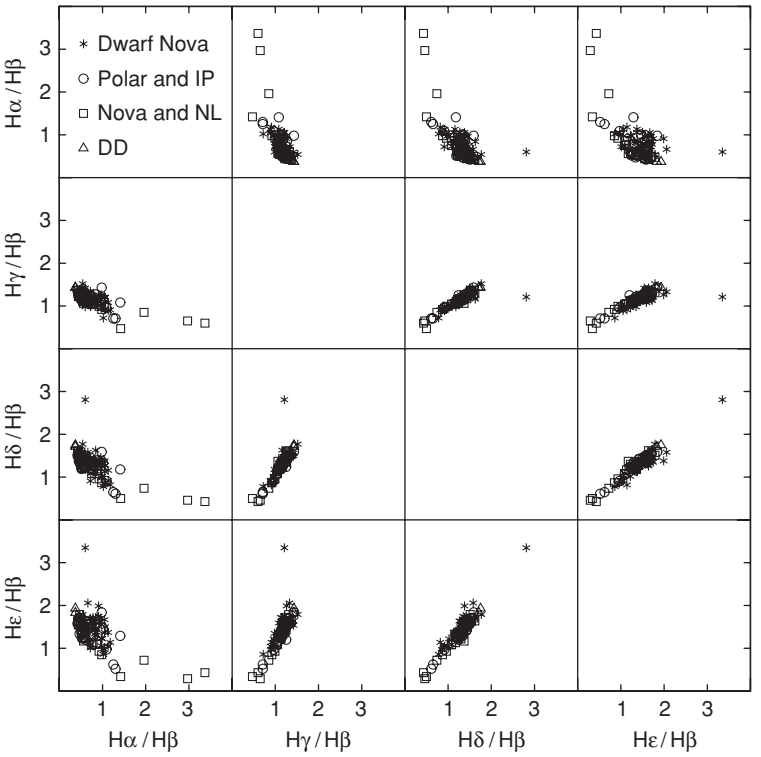

Figure 1 Scatterplot of the emission line data given in Table 1. IP = intermediate polar, NL = nova-like, DD = double degenerate (which are systems containing two white-dwarfs). Individual systems are difficult to identify in general at this scale but four outlying nova and nova-likes and one outlying dwarf nova are obvious. From top to bottom in the Hγ/Hβ versus Hα/Hβ box, the nova and/or nova-likes are RS Oph, T CrB, N Sgr 1962 and V1017 Sgr. The outlying dwarf nova is RU Peg. See text for a discussion of those stars.

The discriminant function that maximally splits the Class 3 groups of dwarf novae versus mCVs is

$$z = -0.583 + 1.125x_1 - 1.229x_2 - 7.812x_3 + 7.757x_4 \quad (3)$$

The value of Wilk's lambda for this function is $\Lambda = 0.791$ with $p = 0.004$. The unit vector $\mathbf{V_3}$ = [0.101 –0.110 –0.702 0.697]^T is normal to the level surface hyperplanes of the discriminant function for Class 3. Histograms of the distribution of the values for the Class 3 discriminant function are given in Figure 3. The angle between $\mathbf{V_2}$ and $\mathbf{V_3}$ is 6.8°.

The direction first principal component (direction of maximum data variance) is given by the unit vector $\mathbf{V_1}$ = [–0.441 0.510 0.530 0.514]^T. The direction of a least squares line fit through the data in the 4D scatterplot space is given by the unit vector $\mathbf{V_4}$ = [–0.816 0.236 0.339 0.405]^T and the angle between $\mathbf{V_1}$ and $\mathbf{V_4}$ is 29.8°. The angles between the first principal component direction, $\mathbf{V_1}$, and the two discriminant function directions, $\mathbf{V_2}$ and $\mathbf{V_3}$, are 95.6° and 96.6° respectively.

3.2 Line Characteristics of Theoretical Models

3.2.1 Optically Thin Photoionized Plasmas

It is useful to consider emission from photoionized gas, which may be present in a disc, accretion stream or in surrounding nebulousity left over from previous nova eruptions since it is expected that all CVs experience periodic nova eruptions (Warner 1995). For this purpose the photoionization-recombination models in Osterbrock (1989) are relevant and the resulting scatterplot points are given in Figure 4. After excitation via boundary layer X-ray and UV illumination, optical recombination line emission may be modelled under two situations known as Case A, in which all emitted photons escape from the gas, and Case B, where the optical depth is high enough to convert every Lyman-line photon into lower-series photons plus either a Lyman α photon or two continuum photons through scattering. For Case B the assumed electron number density, N_e, is relevant, and the models illustrated in Figure 4 assume $N_e = 10^2$, 10^4, and 10^6 cm^{-3}. It may be seen that the dependence of the photoionization caused Balmer line ratios on temperature and gas density is relatively weak but that significantly non-flat Balmer decrements are predicted. In addition, the trend of scatterplot positions for higher density gas versus lower density gas for the photoionization models is in the same general direction as the two disc models described below with, for example, the higher density cases being positioned in the upper left hand part of the scatterplot and the lower density discs in the lower right hand part for the Hα/Hβ versus Hγ/Hβ (abscissa versus ordinate) scatterplot.

3.2.2 Accretion Discs with Optically Thin Continuum

Williams (1980) presented calculations of H Balmer lines from accretion discs, with an outer region optically

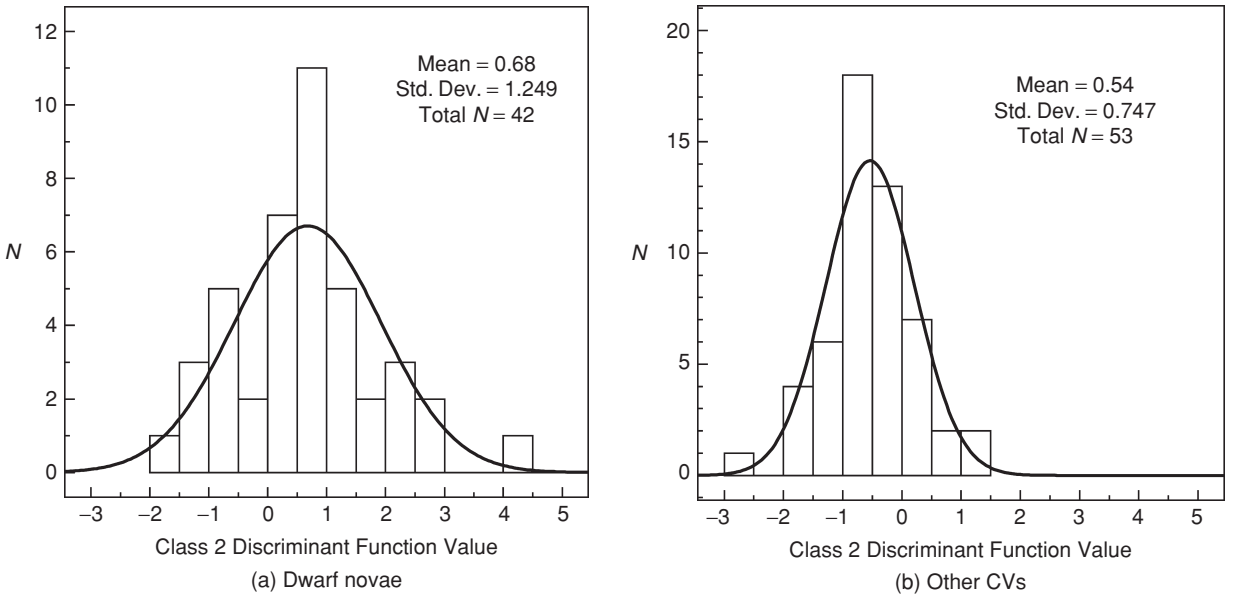

Figure 2 Histograms of discriminant function values for discriminating dwarf novae from all other CVs. All other CVs include nova in low states and mCVs. (a) Dwarf novae. (b) Other CVs including polars, IPs, nova remnants and nova-like variables. Overlain on each histogram is a normal curve having the same mean and standard deviation as the histogram. N = number of systems.

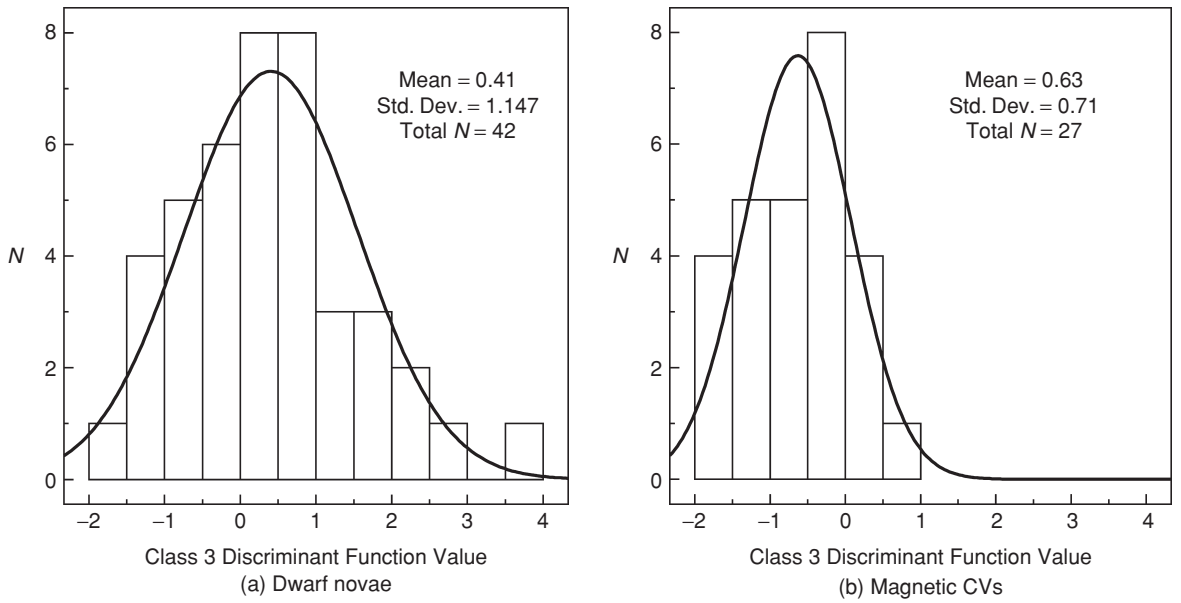

Figure 3 Histograms of discriminant function values for discriminating dwarf novae from mCVs. (a) Dwarf novae. (b) MCVs including polars and IPs. Overlain on each histogram is a normal curve having the same mean and standard deviation as the histogram. N = number of systems.

thick to the lines but optically thin to the continuum. The emission lines arise directly from a hot disc instead of from a disc chromospheric surface layer heated by X-ray and UV radiation from the accretion boundary layer near the white-dwarf surface. An α-disc prescription is used to determine the radial density and temperature profile, and the line-centre intensities are given by the local Planck function at the relevant frequencies. Williams' (1980) calculations predict that the position of a line in the emission line ratio scatterplot space depends on the disc mass flow rate $\dot{M}$ (Figure 4). The predicted equivalent width of the Hβ line, EW(β), varies from 0.2 Å for $\dot{M} = 10^{-9}$ $M_\odot$ yr^{-1} to 65 Å for $\dot{M} = 10^{-12}$ $M_\odot$ yr^{-1}. The cases represented in Figure 4 are for a disc of outer radius $r_d = 4 \times 10^{10}$ cm and a white-dwarf of radius $R_1 = 6 \times 10^8$ cm and mass $M_1 = 1.0$ $M_\odot$. The assumed disc radius r_d corresponds to 1/3 the separation of two 1 $M_\odot$ stars having an orbital period of 4 hr.

We note that in order to have the assumption of an optically thin continuum satisfied, the accretion rate of the system must not greatly exceed 10^{-10} $M_\odot$ yr^{-1}. Most

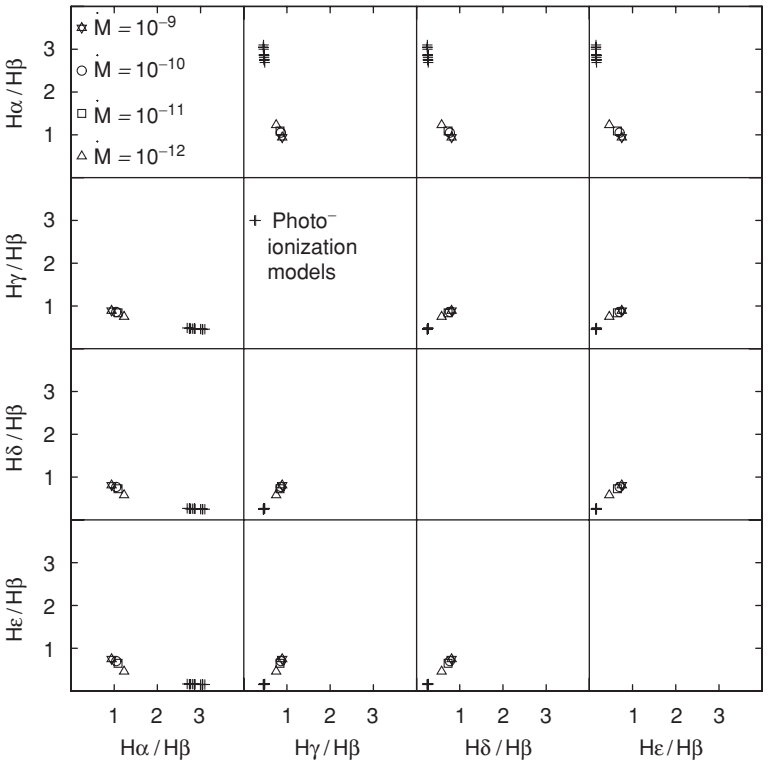

Figure 4 Photoionization and LTE optically thin accretion disc models. The photoionization emission models are from Osterbrock (1989) and both Case A and Case B models (see text) are plotted. The Balmer emission line ratios from the LTE radiative transfer calculations assume an α-disc model with various mass transfer rates (Williams 1980). $\dot{M}$ is given in $M_\odot$ yr^{-1}.

CVs are, however, observed to have higher accretion rates, so that models assuming an optically thin continuum are not always applicable.

3.2.3 Non-LTE Emission from Isothermal Medium

The predictions of a non-LTE model as computed by Williams (1991) are summarized in Figure 5. The model assumes an isothermal horizontally infinite disc (Williams & Shipman 1988) with a Gaussian dropoff in density with vertical height from the midplane. The H number density N_0 [cm^{-3}] represents the value in the disc midplane, which is generally a monotonic function of disc mass flow rate. The position of the line ratios on the scatterplot are more influenced by the value of N_0 than by the temperature, with the higher density discs being represented in the upper left hand part of the scatterplot and the lower density discs being represented in the lower right hand position. This trend is similar to the LTE models in Figure 4 where systems with high accretion rates are positioned in the upper left hand part of the Hα/Hβ versus Hγ/Hβ (abscissa versus ordinate) box and the lower mass flow rates are represented in the lower right hand location. However, the range of predicted line ratios are wider for this model, especially for Hα/Hβ. In particular, the model predicts significantly non-flat Balmer decrements. Additionally, for disc models with temperatures between 15 000 K and 8 000 K, the predicted EW(β) is much larger than for the optically thin LTE models. The predicted EW(β) varies strongly as a function of N_0, going from $\sim$200 Å for log N_0 = 11.5 to $\sim$10 Å for log N_0 = 14.0.

3.2.4 Chromospheric Model

The prediction of Balmer line absolute strengths from disc chromospheres is made difficult because of the strong dependence of the underlying continuum contributions on the disc model (Ferguson 1997). However models of disc chromospheres have been made because of the probable existence of such chromospheres. Situations where Q/κ is a decreasing function of temperature, where Q is the energy generation and κ is the Rosseland mean absorption coefficient in an atmosphere, can lead to an instability and a discontinuity in temperature in which the temperature jumps higher as the pressure decreases (Shaviv & Wehrse 1986). These are situations that lead to the formation of chromospheres and/or coronas. Such a situation was shown to exist in α prescription accretion disc models by Adam et al. (1988). Given the probable existence of disc chromospheres, Williams (1995) modelled emission from chromospheres over α-disc models using radiative transfer methods, particularly computations using the Feautrier method, similar to those used in the non-LTE isothermal models described in section 3.2.3 above. The Balmer line emission ratios predicted by Williams' (1985) chromosphere models are summarized in Figure 6. The associated predicted EW(β) values are small and vary from 1.02 Å in model 6 to 32.27 Å in model 11.

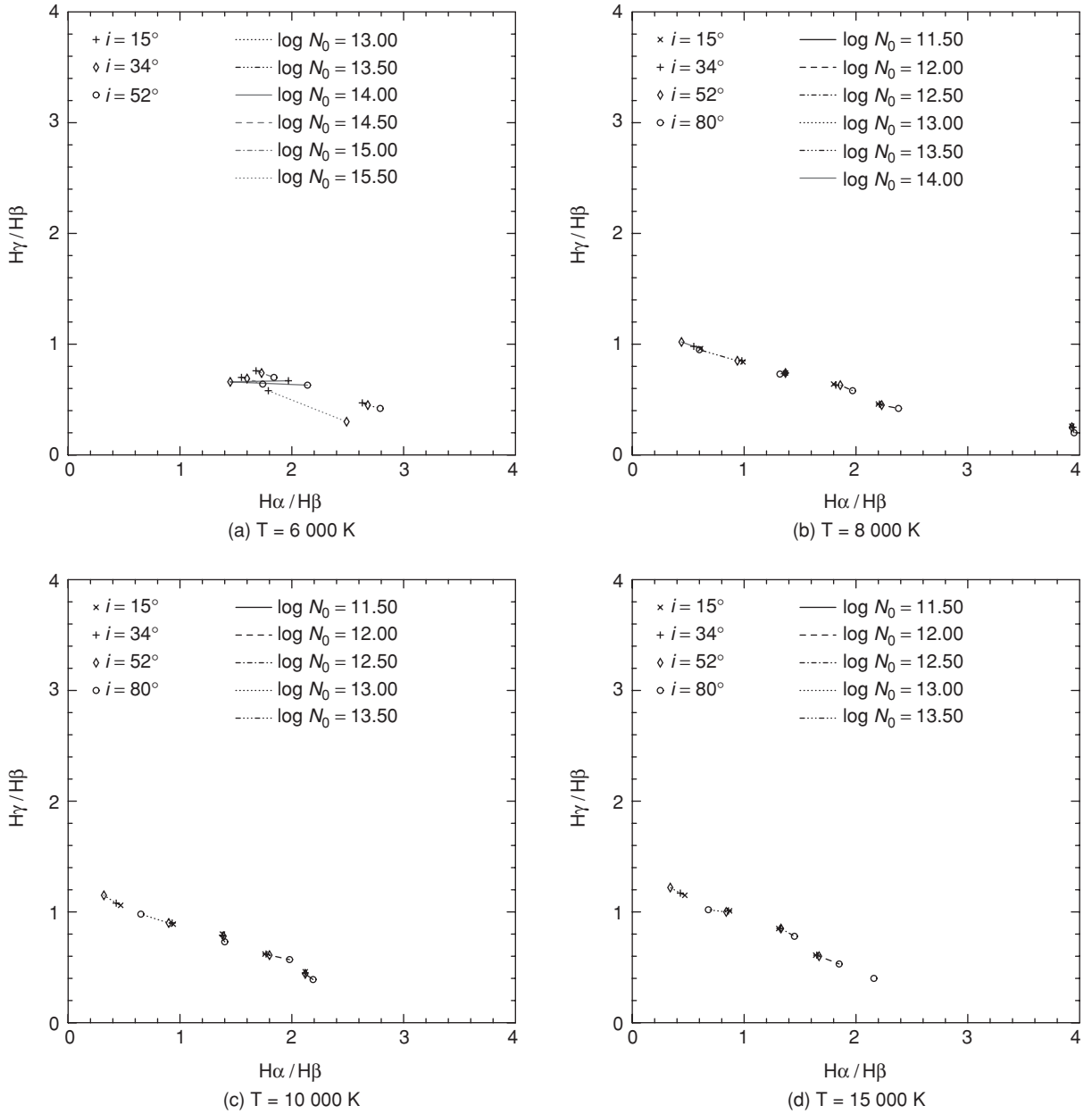

Figure 5 Scatterplots of Hα/Hβ versus Hγ/Hβ values from the non-LTE calculations of Williams (1991). Hydrogen number density, N_0, units are cm^{-3}; i is disc inclination.

4 Discussion

Echevarría (1988) has compiled emission line data for CVs from several sources and produced a number of relevant scatterplots but did not subject the data to any formal multivariate statistical analysis. Echevarría reported a good fit (unquantified) of the H Balmer emission line ratio scatterplot with an LTE gas slab model computed by Drake & Ultrich (1980) in which position along roughly the principal component direction found in our present analysis depended only on disc temperature. Sources positioned further from the Drake & Ultrich model line in the H Balmer emission line ratio scatterplot space were found by Echevarría to have narrow Hβ equivalent widths. Here we have taken H Balmer emission line data from a single survey (Williams 1983) and performed PCA and discriminant function analysis.

The two multivariate analysis methods that we used literally give orthogonal results which, as we have indicated in Section 2, would be expected if the discriminant function were found to be statistically significant. The first principal component direction is roughly in line with a least squares line fit through the 4D scatterplot data; the direction of the least squares line, $\mathbf{V_4}$, is 29.8° from the first PCA direction, $\mathbf{V_1}$. The discriminant function directions $\mathbf{V_2}$ and $\mathbf{V_3}$, on the other hand, form angles of 95.6° and 96.6°, respectively, with

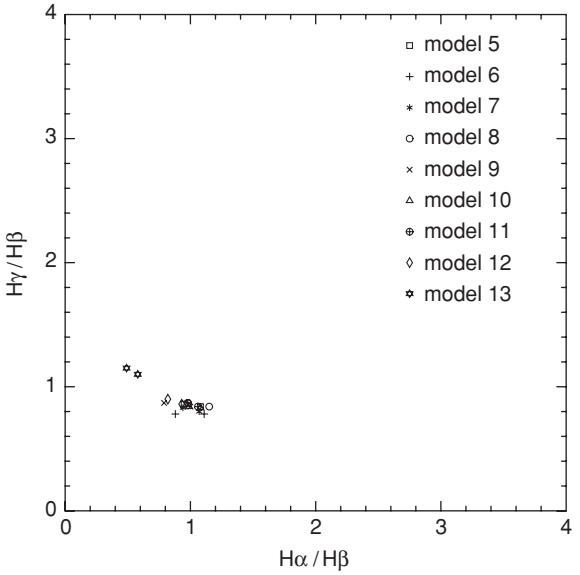

Figure 6 Chromospheric models of Williams (1995). For each model number, from 5 to 13, two outer disc radii are considered, 10^{10} and 2×10^{10} cm with the model position moving from the upper left to lower right as the radius is increased. The assumed disc mass flow rate is 10^{14} g s^{-1} for models 5, 7, and 8, 10^{15} for models 6, 9, and 12. $10^{13.5}$ for models 10 and 11, and $10^{15.5}$ for model 13. The boundary layer luminosity, which photoionizes the chromospheric gas, is taken as compatible with the disc mass flow rate, except for models 8, 9, and 11 where the boundary layer luminosity is that corresponding to 10 times the disc mass flow rate. Finally the α disc viscosity parameter is assumed to be 1.0 for all models except for models 7, 12, and 13 where α is assumed to be 0.5, 10.0, and 100.0 respectively.

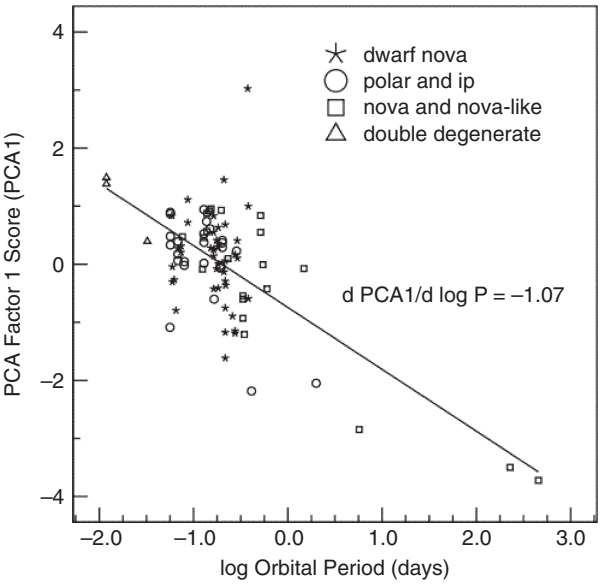

Figure 7 Correlation of the log of the orbital period, as given by Downes et al. (2001), with the first principal component value. Shown is the least squares line fit through the data; a fit having a correlation of –0.664.

the first PCA direction. Further, the discriminant function directions are nearly orthogonal to the second and third principal component directions and are most nearly aligned with the fourth principal component direction (within $\sim 15^\circ$ — there is no statistical or geometrical reason for the discriminant function direction to match any of the principal component directions; its direction is strongly dependent on the direction of the difference between the mean vectors of the groups). The difference between the first principal component direction and the discriminant direction suggests that the physical processes responsible for the majority of the variance of the data (82% of the overall variance is in the first principal component direction) are different to those that separate dwarf nova from other CVs. The first principal component direction reflects the fact that the Balmer decrement changes in a systematic way from one system to the next. We also note that the 'decrements' become 'increments' for many systems (cf. Figure 1 where it may be seen that many ratios are greater than one for Hγ/Hβ to Hε/Hβ). None of the models considered here (or any model that we are aware of) predict such 'increments' (cf. Figures 4–6).

Patterson (1984) shows a good correlation for low-mass interacting binaries between the orbital period $P_{\rm orb}$ and the mean mass transfer rate $\langle \dot{M} \rangle$ from the secondary to the primary, as determined by a variety of methods, and presents an empirical relation

$$\langle \dot{M} \rangle = 5.1^{+3}_{-2} \times 10^{-10} P_4^{3.2\pm0.2}\, \mathrm{M}_\odot \mathrm{yr}^{-1}, \qquad (4)$$

where P_4 is $P_{\rm orb}/4$ with $P_{\rm orb}$ given in days. Although mass transfer rates for individual systems are known to vary widely from the rate given in Equation (4),we can apply it to the data set of Williams (1983) to see whether any average driven trends can identified. Using $P_{\rm orb}$ as given by Downes et al. (2001), $\dot{M}$ was computed using Equation (4) and the correlation between $\dot{M}$ and the first principal component data values determined; a correlation of –0.436 ($p = 1 \times 10^{-5}$, two-tailed) was found. More directly, the correlation between log $P_{\rm orb}$ and the first principal component data values was found to be –0.664 ($p = 5 \times 10^{-13}$, two-tailed), a result which may by appreciated in Figure 7. The implication is that the majority of the variance in the data along the first principal component direction is due to variance in mass transfer rate. However, from inspection of Figure 7, it appears that this conclusion may be strongly influenced by the T CrB systems which are known to have high mass flow rates (Warner 1995). Removal of the T CrB systems only reduces the correlation between the first principal component and log $P_{\rm orb}$ to –0.452 ($p = 8 \times 10^{-6}$, two-tailed) so the influence of the T CrB systems did not overwhelmingly bias the correlation.

The ordinate of the graph shown in Figure 7 roughly follows the direction (within 29.8°) of the line along which the data points lie in the 4D emission line ratio scatterplot space. The LTE model, as shown in Figure 4, predicts a mass flow rate that increases as the first principal component coordinate increases. This variation is incompatible with $\dot{M}$ increasing with $P_{\rm orb}$, as given by

Equation (4) for example, and with an increase of P_{orb} with a decreasing first principal component coordinate as shown in Figure 7. A possible reason for the opposing correlations between $\langle \dot{M} \rangle$ and the first principal component coordinate seen in the data and between $\dot{M}$ and the first principal component seen in the LTE models is that the LTE models may only be applicable to individual systems as an approximation when $\dot{M}$ varies because of disc instability and cannot be generalized to CV population behaviour where $\langle \dot{M} \rangle$ varies because of orbital period differences.

Discriminant function analyses based on either comparing dwarf novae with all other CVs or on comparing dwarf novae with magnetic CVs lead to similar separations. The mean discriminant function values for dwarf novae are statistically significantly different from other CVs and, from inspection of Figures 2 and 3, the variance of H Balmer emission line discriminant function values is wider for dwarf novae than for other CVs.[1] Since the discriminant function directions are nearly orthogonal to the first principal component direction, the physical processes that lead to the segregation of dwarf novae from other CVs in the discriminant function direction appear not to be related directly to the differences in mass transfer rate if Equation (4) is taken as true. Supporting this conclusion, we additionally found no significant correlation between $\langle \dot{M} \rangle$, as given by Equation (4), and discriminant function values ($p > 0.75$, two-tailed) or between log P_{orb} and discriminant function values (two-tailed $p > 0.75$ with the marginal exception of a correlation of –0.213, with two-tailed $p = 0.041$, between log P_{orb} and the Class 2 discriminant function values — but any kind of correction for multiple comparisons makes this correlation non-significant).

Visual comparison of Figure 1 to Figure 4 suggests that the main source of H Balmer emission from T CrB systems is from nebula-like photoionization plasmas. Such photoionization may occur in the nebulousity surrounding the binary star, left behind from the recurrent nova activity. The scatterplot values for the four T CrB systems represented in the dataset are, however, more widely spaced than the values given by the theoretical calculations. This increase in spacing may be caused by the underlying absorption spectrum of the giant star which might tend to reduce Hα/Hβ. An exception is RS Oph which shows line ratio values consistent with a low temperature (5000 K) Case A (optically thin) situation.

Possible sources of H Balmer emission in polars include the stream between the secondary and the (magnetic) threading region, gas falling down the magnetic field line, the heated surface of the stream close to the accretion zone, or a reprocessing of high energy accretion radiation on the surface of the secondary star. Since polars possess no disc and all other CVs are likely to possess accretion discs of some sort, one would think that difference would discriminate polars from all other CVs in the 4D scatterplot space examined here. But that is not the case. Dwarf nova discs, however, may be distinguished from other CV discs in that the disc is unstable, and they undergo thermal cycling which leads to outbursts. The differences in H Balmer emission line ratios between polars and non-dwarf nova CVs are smaller than the differences between dwarf novae and all other CVs, at least in the direction of the discriminant functions found here. Therefore, there appear to be physical processes occurring in the accretion discs of dwarf novae that are different from those happening with the other CV types and it appears that there is a wide variation in the manner in which those unique dwarf nova processes occur. The obvious interpretation is that, since the states of the accretion discs in dwarf novae are continuously changing, our data includes discs at random phases between their last outburst and the next one.

Echevarría (1988) speculated that variation normal to our principal component direction was due to variation in the equivalent width of the Hβ line, EW(β). To test the hypothesis that variation along the Class 2 discriminant function was related to equivalent width, we computed the correlation of the Class 2 discriminant function values with EW(β), as given by Williams (1983), and found a correlation of $r = 0.422$ ($p = 1 \times 10^{-4}$, two-tailed). This correlation is illustrated in Figure 8.

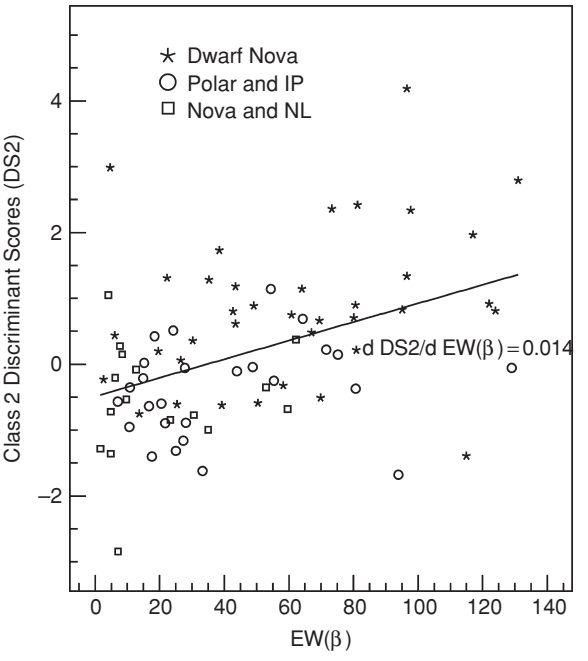

Figure 8 Correlation of the equivalent width of Hβ, EW(β), as given by Williams (1983), with the value of the discriminant function based on Class 2. Shown is the least squares line fit through the data; a fit having a correlation of 0.422. No EW(β) values for AM CVn stars were given by Williams.

[1] It should be noted that interstellar reddening is a possible source of variance for all groups, but this should not affect the *difference* in variances either between dwarf novae and other CVs or between dwarf novae and magnetic CVs.

This correlation, in turn, implies a wide variance in EW(β) of dwarf novae in the dataset, relative to other CVs, from the wide variance of their discriminant function values (see Figure 2). The correlation of EW(β) with the first principal component value is insignificant at $r = -0.016$ ($p = 0.891$) indicating that the cause of EW(β) is closely related to the cause of variation in the discriminant function direction. Patterson & Raymond (1985) show that the ratio of X-ray flux (0.2 – 4.0 keV) to optical flux, F_x/F_v, is positively correlated with EW(β) for CVs with accretion discs. If this were true for all CVs then the discriminant function direction would correspond to the relative X-ray intensity of the accretion region on the white dwarf. However, this interpretation is inconsistent with observed $0.001 < F_x/F_v < 10$ for dwarf novae and $3 < F_x/F_v < 300$ for polars (Warner 1995) when the values of the discriminant function as shown in Figure 2 or 3 are considered. In other words, polars tend to have smaller EW(β) than dwarf novae, not larger widths as would be implied by a larger F_x/F_v. The physical processes behind the production of Balmer emission in polars is not a continuous variation of the processes that produce Balmer emission in dwarf novae.

The Doppler width of the Hβ line, DW(β), is weakly correlated with both the Class 2 discriminant function value ($r = 0.325$, $p = 0.006$) and the first principal component value ($r = 0.377$, $p = 0.001$). Therefore factors influencing the DW(β) value, such as broadening due to disc rotation, have no coherent effect on the variation of Balmer emission line ratios in the population of CVs. But the variation in radiative transfer processes that give rise to variation of EW(β) is coherently related to the variation of emission line ratios in our sample of CVs, specifically in the discriminant function direction in which dwarf nova may be distinguished from all other types of CVs. Inspection of Figure 8 reveals that the variation of dwarf nova EW(β) values in the discriminant function direction is much larger that the variation of other CV EW(β) values, which tend to be smaller. This behaviour, of course, is simply a reflection of the behaviour of discriminant function values illustrated in Figure 2. Since all dwarf nova contain unstable accretion discs (Cannizzo et al. 1988) as a primary feature distinguishing them from other CVs, we may speculate that the variation of dwarf nova EW(β) values is due to the variation of physical processes in the disc, perhaps related to thermal cycling in the disc as mentioned earlier.

Echevarría (1988) essentially found variation along what we have defined as the first principal component direction to be a function of temperature while we hypothesized that it is essentially a function of mass transfer rate. The two conclusions are consistent because higher mass flow rates implies higher temperatures in the α-disc model (Frank, King, & Raine 1995). Echevarría found deviation in H Balmer line scatterplot space away from the LTE model of Drake & Ultrich to be related to the equivalent width of the Hβ line. We analogously find, more rigorously, that variation in the Class 2 discriminant function direction, which is roughly orthogonal to the first principal component direction, is correlated with the equivalent width of the Hβ line.

5 Conclusions

Our analysis of hydrogen Balmer lines in CVs shows that the source of variation seen in the principal components analysis is correlated with the binary orbital period, and that the source of variation seen in the discriminant function analysis is correlated with the equivalent width of the Hβ line. Comparing models to the data produces one positive result: The ratios of hydrogen Balmer lines predicted by the photoionized model match the observed line ratios of the T CrB systems. In particular, the emission from RS Oph is consistent with photoionization from a $\sim$5000 K optically thin (Case A) nebula. These systems, with a massive white dwarf and likely progenitors of type Ia supernovae, are hypothesized to be embedded in a nebula produced by the frequent novae outbursts (Warner 1995). Our analysis supports this scenario, as the observed Balmer emissions could originate from a photoionized nebula. Otherwise, the theoretical models considered in this work do not produce the wide range of line ratios along the first principal component direction of the CV dataset. In particular, if we assume that the mass-transfer rate and the period are related by Equation (4), the model of LTE emission from an isothermal medium predicts a correlation between the observed first principal component direction and mass transfer rate opposite to what is observed.

Our analysis showed a wide variance of discriminant function values and a wide distribution of line ratios along the first principal component direction for dwarf novae. In light of the known thermal cycling in the accretion disc, regardless of whether the lines are emitted directly from the disc or are from reprocessed radiation, both the Balmer line ratios and the line equivalent widths would be expected to vary with the dwarf nova outburst cycle. This may be a cause of the wide variance in the discriminant function values and of the wide distribution along the first principal component direction. As far as we are aware, systematic observations of hydrogen Balmer emission lines throughout a dwarf nova cycle have not been reported.

Our analysis shows that the range of Balmer ratios seen along the first principle component direction, including 'inverted' Balmer decrements, cannot be reproduced by the conventional models considered here. The more or less continuous variation of the line ratios from Balmer decrements to Balmer 'increments' for all CVs as a group prevents any clustering of the data that clearly points to a particular single underlying physical process. We therefore conclude that either the emission from different CV sub-classes have different locations (and hence line formation processes) within the system, or there are multiple regions for the

source of hydrogen Balmer lines within a CV. The good matching between the data of T CrB systems and the photo-ionization nebular model supports the former. However, the latter is also likely, given that the UV radiation from the accreting white dwarf can ionize the cooler material in the outer accretion disc, the accretion stream, and the companion star.

Acknowledgments

G.E.S. is supported by a discovery grant from the Natural Sciences and Engineering Research Council of Canada (NSERC). G.E.S. also thanks the MSSL for their hospitality during his visits in 2005 and 2006. Conversations with Laszlo Kiss about T CrB spectra are gratefully acknowledged. K.W. thanks TIARA for their hospitality during his visit there and for support through a Visiting Fellowship. TIARA is operated under Academia Sinica and the National Science Council Excellence Projects programs in Taiwan administrated through grant number NSC 94-2752-M-007-001.

References

Adam, J., Stozer, H., Shaviv, G. & Wehrse, R. 1988, A&A, 193, L1
Cannizzo, J. K., Shafter, A. W. & Wheeler, J. C. 1988, ApJ, 333, 227
Cropper, M. C., 1990, SSRv, 54, 195
Downes, R. A., Webbink, R. F., Shara, M. M., Ritter, H., Kolb, U. & Duerbeck, H. W., 2001, PASP, 113, 764
Drake, S. A. & Ultrich, R. K., 1980, ApJS, 42, 351
Duerbeck, H. W., 1987, SSRv, 45, 1
Echevarría, J., 1988, MNRAS, 233, 513
Ferguson, D. H. 1997, ApJ, 486, 987
Frank, J., King, A. R. & Raine, D., 1995, Accretion Power in Astrophysics, Second Edition, Cambridge University Press, Cambridge
Osterbrock, D. E., 1989, Astrophysics of Gaseous Nebulae and Active Galactic Nuclei, University Science Books, Mill Valley, CA
Patterson, J. 1984, ApJS, 54, 443
Patterson, J. & Raymond, J. C. 1985, ApJ, 292, 535
Rencher, A. C. 2002, Methods of Multivariate Analysis, Second Edition, Wiley-Interscience, NY
Shakura, N. I. & Sunyaev, R. A. 1973, A&A, 24, 337
Shaviv, G. & Wehrse, R. 1986, A&A, 159, L5
Warner, B. 1995, in Cataclysmic Variable Stars (Cambridge: Cambridge University Press)
Williams, R. E. 1980, ApJ, 235, 939
Williams, G. W. 1983, ApJS, 53, 523
Williams, G. A. & Shipman, H. L. 1988, ApJ, 326, 738
Williams, G. A. 1991, AJ, 101, 1929
Williams, G. A. 1995, AJ, 109, 319
Wu, K. 2000, Space Sci. Rev., 93, 611
Wu, K., Cropper, M., Ramsay, G., Saxton, C. & Bridge, C. 2003, ChJAA, 3, Suppl., 235